Gain-driven singular resonances in active core-shell and nano-shell plasmonic particles

Karen Caicedo, Andres Cathey, Melissa Infusino, Ashod Aradian, Alessandro Veltri

Gain-driven singular resonances in active core-shell and nano-shell plasmonic particles

KAREN CAICEDO,[1] ANDRES CHATEY,[2] MELISSA INFUSINO,[3] ASHOD ARADIAN[4] AND ALESSANDRO VELTRI[3,*]

[1]*Univ. Bordeaux, CNRS, IOGS, LP2N, UMR 5298, F-33400 Talence, France*
[2]*Max Planck Institute for Plasma Physics, Boltzmannstr. 2, 85748 Garching, Germany*
[3]*Colegio de Ciencias e Ingeniera, Universidad San Francisco de Quito, Quito,Ecuador*
[4]*Univ. Bordeaux, CNRS, CRPP, UMR 5031, F-33600 Pessac, France, UPR 8641, F-33600 Pessac, France*
[*]*aveltri@usfq.edu.ec*

Abstract: Within the frame of a simple, long-wavelength, quasi-static description, we present a theoretical characterization of the optical response of metal nanoparticles doped with active gain elements in a core-shell (metallic core within an active dielectric shell) and nano-shell (active dielectric core within a metallic shell) configurations. The common feature of these structures is that, adding gain to the system produces an increase of the quality of the plasmon resonance, which becomes sharper and sharper until a singular point, after which, the system switches from absorptive to emissive (nanolaser). We use this aforementioned simple model to develop a general method allowing to calculate both the expected singular plasmon frequency and the gain level needed to realize it, and to discuss the spectral deformation occurring before and after this singular point. Finally we propose a way to calculate if the singular behavior is reachable using realistic amounts of gain.

The last decade has seen the study of resonant plasmonic nanostructures (including noble metals and active elements), steadily gaining momentum within the field of plasmonics while attracting interest in both optoelectronics and nanotechnology due to the variety of the possible applications: nano-resonators in noble metals are, in fact, good candidates for the realization of visible-range metamaterials, where the embedding of optical gain (organic dye molecules or nanocrystals) is possibly the most promising strategy to circumvent the high level of losses they present at these frequencies [1–16], which are, just to mention an example, the primal reason for which the realization of metamaterial based cloaking devices [17–19] at visible frequencies have practically been put aside. Moreover, metallic nanostructures with gain elements are nanoscale sources of strong optical fields; this intriguing feature, culminating in the conception of the SPASER, widened their potential applicability to nanoscale lithography, probing, microscopy and more [20–23]. In the zoo of proposed nanostructures, a prominent role is played by core-shell and nano-shell nanoparticles, for they are controllable and stable plasmonic structures including all features needed for diverse optoelectronic applications [24–27], and they are obtainable in large numbers via nanochemical synthesis [28, 29].

In a previous work [30], we studied the simpler situation of a single, homogeneous metallic nanoparticle immersed in a gain medium; focusing on the plasmonic response, with its amplification and distortions. In that study we have shown that new types of responses arise as the gain level is modified and we emphasized striking differences between gold and silver nanoparticles: when silver is used, the behavior is rather straightforward, with an increasing quality of the plasmon resonance as the amount of gain elements is increased towards the singular point; in gold structures (due to the higher loss associated with the interband transition), the situation is richer, and produces increasingly distorted spectra as the gain increases culminating in the appearance of a "conjugate" plasmon which arise as a Fano-type interference between the plasmon and

the gain resonance curve. This new behavior shows one particularly attractive property from the application standpoint: at the plasmon frequency, the real response is maximal, and losses are close to zero. One of the main objectives of this work is the use of the aforementioned approach for the description of the behaviour of systems experimentally achievable such as gain functionalized core-shell and nano-shell nanoparticle.

The previous model hypothesized an infinite active media surrounding the nanoparticle, uniform in density of molecules and pumping rate. If not completely unrealistic, this system is experimentally unpractical to the least, especially for application requiring a single nanoparticle and not a population. Moreover, we believe that is definitely interesting to verify if the more appealing features of the deformed spectra survive when relaxing the infinite/uniform gain media approximation. For these reasons, we propose here a model for gain embedded nanoparticles in the core-shell (with metal core and a dielectric shell including gain elements) and nano-shell (with metal shell and a dielectric core including gain elements) configurations. By introducing the aspect ratio ρ as the ratio between the internal and the external radius of these structures and a parameter G that will be defined later, which accounts for the quantity of gain in the system, we will explore the $[\rho, G]$ parameter space looking for all of the interesting behaviors discussed in our previous work and more.

1. Core-shell and nano-shell geometries

We consider a single spherical nanoparticle (NP) whose core, of a relative permittivity ε_c, is defined by the inner radius r_1; this core is covered by a coating shell of permittivity ε_s located in the space between r_1 and the external radius r_2 of the nanoparticle. The whole system is immersed in a dielectric host medium with relative permittivity ε_h. In the quasi-static limit, where the size of the nanoparticle is enough smaller than the exciting wavelength, the dipolar polarizability α of such a NP is classically given as [31]:

$$\alpha(\omega) = 4\pi r_2^3 \varepsilon_h \frac{(\varepsilon_s - \varepsilon_h)(\varepsilon_c + 2\varepsilon_s) + \rho^3(\varepsilon_c - \varepsilon_s)(\varepsilon_h + 2\varepsilon_s)}{(\varepsilon_s + 2\varepsilon_h)(\varepsilon_c + 2\varepsilon_s) + 2\rho^3(\varepsilon_s - \varepsilon_h)(\varepsilon_c - \varepsilon_s)} \quad \text{where } \rho = \frac{r_1}{r_2}. \tag{1}$$

The difference between the core-shell and the nano-shell, here resides in the definition of the permittivities ε_c and ε_s: by using a metal permittivity for ε_c and a gain assisted dielectric one for ε_s equation 1 represent a core-shell nanoparticle, by doing the reverse it describes a nano-shell one. The polarizability of a nanoparticle couples the total dipole moment $\mathbf{p}$ with the local electric field $\mathbf{E}_{loc}$ as $\mathbf{p} = \alpha\varepsilon_0\mathbf{E}_{loc}$ and it is related to the absorbance, the effective permittivity and all the nano and mesoscopic electromagnetic parameters of interest. For this reason it constitutes a reference for the most common optical characterizations.

In the calculations we will carry out in this article, all material permittivities will be denoted as $\varepsilon = \varepsilon' + i\varepsilon''$, with ε' (resp. ε'') the real (resp. imaginary) part. We follow the optics convention: losses correspond to $\varepsilon'' > 0$, and gain to $\varepsilon'' < 0$.

The metal dielectric permittivity ε_m as a function of the angular frequency ω, is interpolated from the Johnson & Christy dataset [32] for gold and silver, and always displays a positive imaginary part $\varepsilon''_m(\omega)$ due to Ohmic losses.

The active gain medium is modeled using a single Lorentzian emission lineshape:

$$\varepsilon_g(\omega) = \varepsilon'_g(\omega) + i\varepsilon''_g(\omega) = \varepsilon_b + \frac{G\Delta}{2(\omega - \omega_g) + i\Delta}, \tag{2}$$

where ε_b is the real, positive permittivity of the background dielectric medium embedding the gain elements (emitters such as dye molecules, quantum dots, etc.), Δ sets the emission bandwidth and ω_g is the central frequency of the emitters. These gain elements are assumed to be externally pumped at some (absorption) frequency located sufficiently far away from the plasmon resonance.

The important quantity G represents the global level of gain in the amplifying medium and is taken as a real, positive quantity. The higher the gain level in the system, the more positive the value of G gets.

To provide gain and compensate for the losses in the metallic parts, $\varepsilon_g''(\omega)$ is indeed negative, and the maximum of emission is obtained for $\omega = \omega_g$ with opposite sign to the parameter G: $\varepsilon_g''(\omega_g) = -G < 0$.

The gain level G is related to microscopic quantities as follows (see section 6 for details):

$$G = \frac{2\mu^2}{3\hbar\varepsilon_0\Delta} n\tilde{N} > 0, \tag{3}$$

where μ is the transition dipole moment of the emitters, $\hbar$ the reduced Plank constant, n the volume density of gain elements, and $\tilde{N}$ the population inversion (i. e. the pumped fraction of the of the gain elements population). In this article, we will be considering the response of the system to variations in the gain level G: once a specific dye is chosen (i.e., μ and Δ are set), these variations can be obtained either by changing the density of emitters n within the gain region of the nanoparticle, or, for a given density, by modifying the pump power (which changes $\tilde{N}$). The latter is obviously more practical but gives access to a limited range of G values, since the inversion population rapidly saturates to a maximum. Changes in the density of gain elements allow to reach higher gain values by packing more emitters, although there are also limitations, as discussed in section 6.

Equation 2 is widely used and accepted as a way to model gain media [16, 27, 33–36], but in the context of nanolasing, it indeed represents a strong approximation: this is presupposing that *(i)* the system is capable of reaching a steady state of emission; *(ii)* the gain medium can be described as a homogeneous medium, with a permittivity ε_g. None of these is obvious, since emissive states are in essence dynamical, and described *via* time and space-dependent equations involving the population densities of various electronic levels. In a previous work [37], we studied the emission of a nanoparticle in a infinite gain medium, using a detailed dynamical model based on the optical Bloch equations: we found that, as long as the system remains lossy (passive) for some frequency ω (i.e., the imaginary part of the polarizability is positive, $\alpha''(\omega) > 0$), the steady-state description of the gain medium holds at that frequency. Where the system becomes emissive with $\alpha''(\omega) < 0$, however, we found that the response in the gain medium becomes non-linear and depends locally on the spatially-varying intensity of the electrical field, so that a simple permittivity-based description similar to equation 2 becomes irrelevant.

Therefore, we emphasize strongly that in what follows, one should exercise caution in reading charts presenting the evolution of, e.g., the polarizability versus the level of gain G: the simplified description put forward in this article works reliably only when $\alpha''(\omega) > 0$, and enables us, in particular, to calculate the response of the nanoparticle up to and at the singularity point. Beyond the singularity point, all lasing states, where $\alpha''(\omega) < 0$, will not be describable using this formalism (the corresponding areas in charts will be identified using a grey shading).

2. Singular resonance

A lot of the most exciting applications require the system to emit and while (as we just discussed) the precise phenomenology of the emissive (lasing) states of the nanoparticle is outside the possibilities of this model, we can still use it to calculate the threshold gain G_{th} needed for the system to start emitting. In all but a few exceptional cases (see further), the switch between absorption and emission behaviours happens when the denominator of equation 1 vanishes and a singularity is produced. Since the denominator is different for core-shells and nano-shells, we

get two conditions:

$$(\varepsilon_m + 2\varepsilon_h)(\varepsilon_g + 2\varepsilon_m) + 2\rho^3(\varepsilon_m - \varepsilon_h)(\varepsilon_g - \varepsilon_m) = 0 \qquad \text{for nano-shells,} \tag{4}$$

$$(\varepsilon_g + 2\varepsilon_h)(\varepsilon_m + 2\varepsilon_g) + 2\rho^3(\varepsilon_g - \varepsilon_h)(\varepsilon_m - \varepsilon_g) = 0 \qquad \text{for core-shells;} \tag{5}$$

solving for ε_g, both conditions can be reduced to the form:

$$\varepsilon_g(\omega) = F(\rho, \omega), \tag{6}$$

where the function $F(\rho, \omega)$ is defined as:

$$F(\rho, \omega) = \varepsilon_m \frac{2\varepsilon_m(\rho^3 - 1) - 2\varepsilon_h(\rho^3 + 2)}{\varepsilon_m(2\rho^3 + 1) + 2\varepsilon_h(1 - \rho^3)}, \tag{7}$$

for the nano-shell structures, and

$$F(\rho, \omega) = \frac{\sqrt{(\varepsilon_h - \varepsilon_m)^2[4\rho^3(\rho^3 + 1) + 1] + 3\varepsilon_h[\varepsilon_h(4\rho^3 + 5) + 2\varepsilon_m(10\rho^3 - 1)]}}{4(1 - \rho^3)} + \\ - \frac{\varepsilon_h(\rho^3 + 2) + \varepsilon_m(2\rho^3 + 1)}{4(1 - \rho^3)} \tag{8}$$

for the core-shell structures. Note that the function F depends only on the structural parameters of the nanoparticle (materials and aspect ratio), but not on the gain level in the system. Note also that, while equation 4 is linear in ε_g, equation 5 is quadratic: this means that a second solution (other than the one presented in equation 8) exists in principle for core-shells; however, it produces non-physical effects such as negative values for G_{th}, so that it can be safely dismissed.

Condition 6 not only defines the threshold gain G_{th}, i.e. the minimal gain in the system necessary to obtain a singular plasmon, it also yields the singular resonance frequency ω_{sp}; in both the core-shell and the nano-shell case, by substituting expression 2 in equation 6, one can easily obtain the following relation:

$$\frac{G_{th}\Delta}{4(\omega_{sp} - \omega_g)^2 + \Delta^2} = \frac{F(\rho, \omega_{sp}) - \varepsilon_b}{2(\omega_{sp} - \omega_g) - i\Delta}, \tag{9}$$

We note that the left-hand side of equation 9 is real, while the right-hand term is complex, so that the imaginary part of the right-hand term must be zero:

$$\Delta\,[F'(\rho, \omega_{sp}) - \varepsilon_b] + 2F''(\rho, \omega_{sp})(\omega_{sp} - \omega_g) = 0 \tag{10}$$

where F' and F'' are the real and imaginary parts of F. This last equation allows to calculate ω_{sp}; once this is known, we can use the real part of equation 9 to calculate:

$$G_{th} = \frac{2}{\Delta}(\omega_{sp} - \omega_g)\left[F'(\rho, \omega_{sp}) - \varepsilon_b\right] - F''(\rho, \omega_{sp}). \tag{11}$$

It should be noted that, when using expression 7 for F (nano-shell), condition 9 is the same as that derived in [38], where it was directly calculated from boundary conditions. It can be also of interest that if one uses $F(\omega, \rho) = \varepsilon_m/2$, the same procedure gives G_{th} and ω_{sp} for a single metal particle in a infinite and uniform gain medium [30].

One can see that both ω_{sp} and G_{th} depend on ρ and on the distance $(\omega_{sp} - \omega_g)$ between the singular plasmon frequency and the gain center position. It is possible to show that the most effective coupling between the gain emission and the plasmon occurs when $\omega_g = \omega_{sp}$, i.e., when the gain emission is centered on the singular plasmon it is feeding; then, the singular plasmon is

obtained with the minimal global level of gain. The further apart one sets ω_g from ω_{sp}, the less effective is the coupling (i.e., the value of G_{th} increases). In the following, we will assume that the gain positioning is always optimal with respect to the resonance ($\omega_g = \omega_{sp}$), including when the value of ρ is changed (in the nano-shell geometry, this leads to a shift of ω_{sp}, and therefore ω_g has to be adjusted accordingly to follow). We stress that this is not a physical prerequisite, but it will make the following discussion much simpler.

Under such optimal gain positioning, equations 10 and 11 simplify into:

$$F'(\rho, \omega_{sp}) = \varepsilon_b \tag{12}$$

$$G_{th} = -F''(\rho, \omega_{sp}), \tag{13}$$

this way making ω_{sp} and G_{th} functions of ρ only.

One final important remark is in order: even in the quasi-static, dipolar regime under consideration, these nanoparticles may in principle support more than one resonance (i. e., there may be several solutions for ω_{sp} in equation 10). This is especially true for the nano-shell geometry, which is known for supporting symmetric and antisymmetric modes [39]. In the following, we always chose to focus on the most intense resonance only, which is the one requiring the lowest amount of gain to reach singularity and be driven to emission: this is the most relevant situation to consider for the means of practical feasibility of a plasmonic nanolaser. (In the case of a nano-shell system, this corresponds to the symmetric resonance.)

3. Gain threshold and singular frequency

In the previous section, we discussed how one can calculate the singular resonance frequency ω_{sp}, using equation 12, as a function of the aspect ratio ρ. In figure 1, we present the results of this calculation for silver (fig. 1a) and gold (fig. 1b). We shall also assume here and for the rest of the article that the background material hosting the gain elements in the nanoparticle is silica ($\varepsilon_b = 2.1316$) and the external medium is water ($\varepsilon_h = 1.769$).

Here one can see that in the core-shell configuration, the singular resonance frequency is basically constant (black line): this should be understood because it essentially reflects the position of the plasmonic resonance of the metallic core as ρ is changed, which is well-known to be mostly insensitive to size in the quasi-static regime of polarizability we considered. In contrast, in the nano-shell configuration (magenta line), ω_{sp} redshifts as ρ increases: this is also expected, since this resonance reflects mostly the symmetric mode of the nanoshell [39].

It is also worth stressing again that, once the value for ρ is decided, the singular resonance center-line ω_{sp} calculated using equation 12, represents the ideal center-line frequency of the gain permittivity $\varepsilon_g(\omega)$ maximizing the plasmon-gain coupling, which could be interesting from an experimental standpoint.

We have also shown how one can use equation 13 to calculate the minimal amount of gain G_{th} (threshold) needed to produce a singular behaviour in the polarizability of core-shells and nano-shells. In figure 2 we present the results of this calculation for silver (fig. 2a) and gold (fig. 2b), plotting G_{th} as a function of ρ in the core-shell (black line) and the nano-shell (magenta line) geometries. The first thing one can notice is that in both cases the gain threshold needed to produce the singular behaviour is up to an order of magnitude larger for gold than it is for silver. This is expected because, compared with silver, gold is a high-loss metal. Also, for both metals and for both configurations, the larger the metal volume, hence losses (i. e. larger ρ for core-shells and smaller ρ for nano-shells), the bigger the level of required gain G_{th} to drive emission. (Ripples in the graph for silver come from strong measurement uncertainties in the the low-energy range of the Johnson & Christy data [32].)

It is important to mention that the results presented in this section (fig. 1 and fig. 2), only depend on the radius ratio ρ and not on the total nanoparticle volume (i. e. ranging ρ by fixing

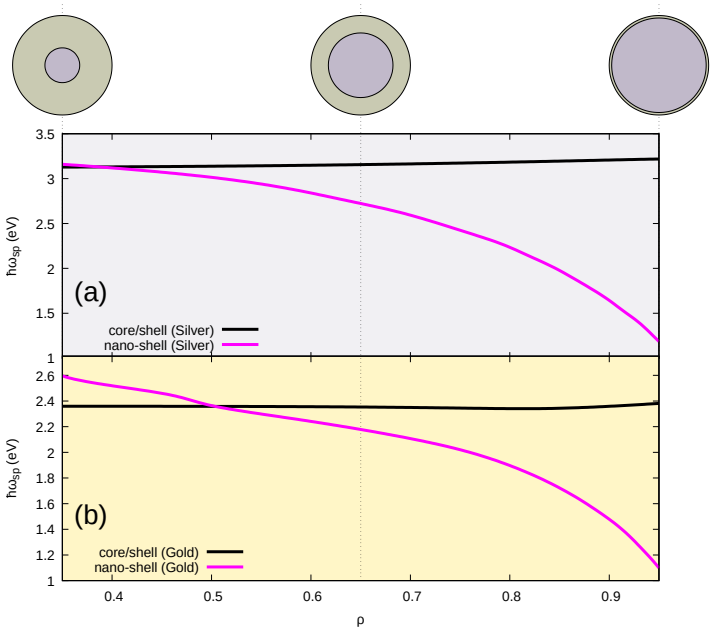

Fig. 1. Singular resonance frequency ω_{sp} as a function of the radius ratio ρ. (a) black: silver core-shell configuration, magenta: silver nano-shell configuration; (b) black: gold core-shell configuration, magenta: gold nano-shell configuration.

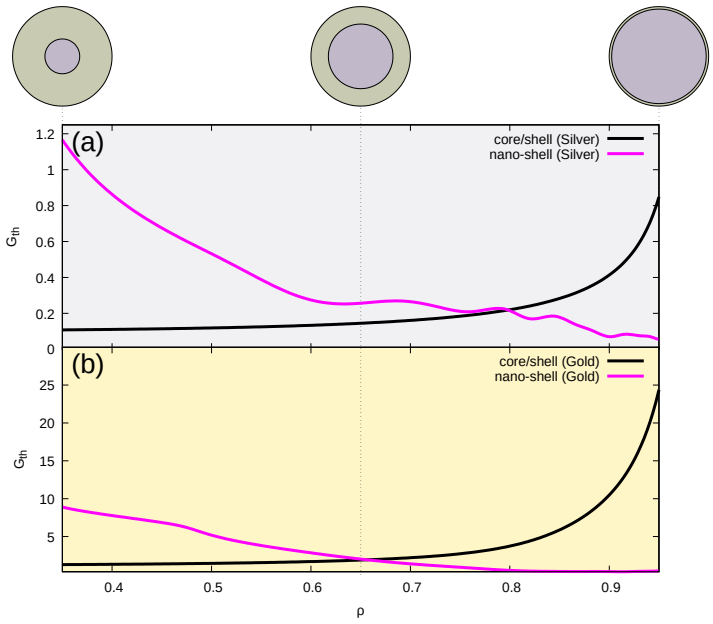

Fig. 2. Gain threshold G_{th} as a function of the radius ratio ρ. (a) black: silver core-shell configuration, magenta: silver nano-shell configuration; (b) black: gold core-shell configuration, magenta: gold nano-shell configuration.

r_1 and changing the shell thickness or fixing r_2 and varying the core volume would produce the same results), because again we restrict ourselves to the quasi-static regime of polarization only. Obviously, for sizes too big to lie in this regime, one would need to take into account the size-dependent dipolar polarizability calculated from the full Mie theory, as well as higher multipoles; the same methodology as exploited here could be applied, in principle, to higher-order polarizabilities, as long as one stays outside the emissive regime (nanolasing) [37].

In the following sections, we will present how the polarizability lineshapes $\alpha(\omega)$ evolve in these structures for different values of ρ different amounts of gain G.

4. Low-loss metal behavior

In figure 3, we present the spectral behavior for a silver core-shell particle with a gain-enriched silica shell, and dispersed in water. In the quasi-static regime, the total particle volume intervenes as a mere scaling factor in eq. 1, and we therefore plot the real and imaginary parts of the reduced polarizability $\alpha(\omega)/(4\pi r_2^3)$ to dismiss such irrelevant size effects. (Note also that we have chosen a realistic value for the emitter's bandwith Δ: $\hbar\Delta = 0.15$ eV.)

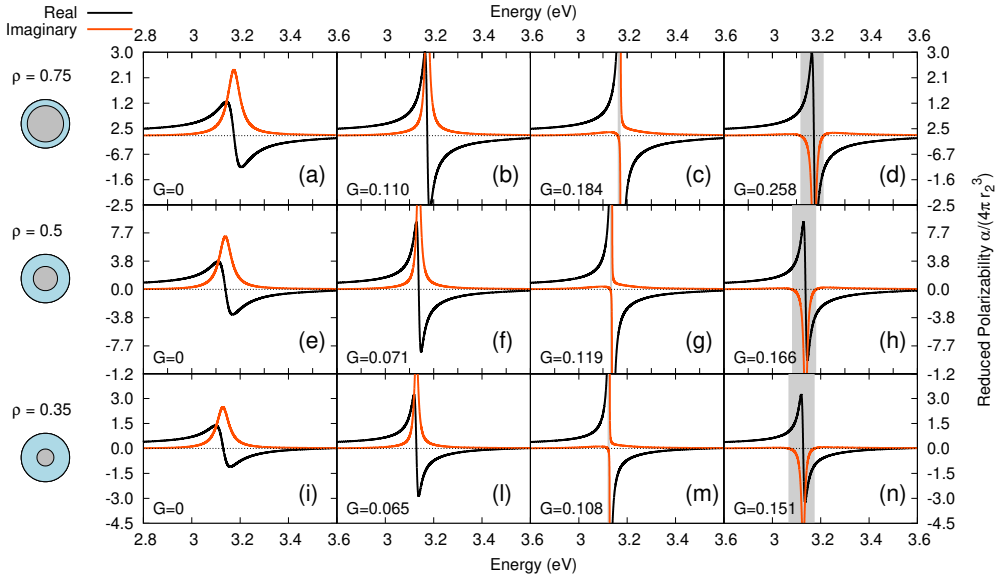

Fig. 3. *Silver core-shell:* Evolution of the plasmon resonance of a 20-nm core-shell nanoparticle embedding a silver-core in a gain-enriched silica shell and dispersed in water. Black curves: real part of the reduced polarizability, orange curves: imaginary part. As gain is increased (from left to right) and for different shell thickness [increasing from up to down] before and after the singular plasmon values [(c), (g), (m)]. Parameters: $\varepsilon_h = 1.769$ (water), $\varepsilon_b = 2.1316$ (silica), $\omega_g = \omega_{sp}$ and $\hbar\Delta = 0.15$ eV. The frequency ranges in which the system becomes emissive ($\alpha''(\omega) < 0$) are highlighted in gray.

The spectra here do not differ much from those found in the case of a single silver particle in a uniform gain medium [30]. Specifically, for every row and from left to right one can see a plasmon of increasing quality and amplitude as the gain level G increases from zero (in fig. 3a, e, i), until the singular point ($G = G_{th}$) is reached (see fig. 3c, g, m). It is important to emphasize here that, for these structures, the imaginary part of the polarizability $\alpha''(\omega)$ becomes negative only for $G \geq G_{th}$, meaning that the singular gain G_{th} indeed represents here the threshold between an absorptive and an emissive regime.

As G increases beyond the singular point, the quality of the plasmon resonance gradually degrades due to excess gain, but it acquires a growing negative imaginary part (see grey-shaded areas in fig. 3d, h, n): as discussed in section 1, this corresponds to a frequency region where our simple model breaks down and where a more complete model allowing for a full spatio-temporal dynamics has to be used [37, 40]. Therefore, all curves in these gray regions, should not be taken literally (for this figure and in all subsequent figures presenting a spectrum). Inside the grey regions, results in the related geometry studied in [37] strongly suggest that an exponential amplification (instability) in the field intensity should occur, yielding appropriate conditions for spasing/nanolasing to appear [20, 23]. (And this is indeed fully confirmed by our more recent work on the specific dynamics of the nano-shell geometry [40]). Therefore, one can consider formula 13 as the simplest, existing way to evaluate the minimal amount of gain necessary to realize nano-emitters out of these structures.

In figure 4, we present the spectral behavior for a silver nano-shell particle embedding a gain enriched silica core and dispersed in water. There are two main advantages here, compared

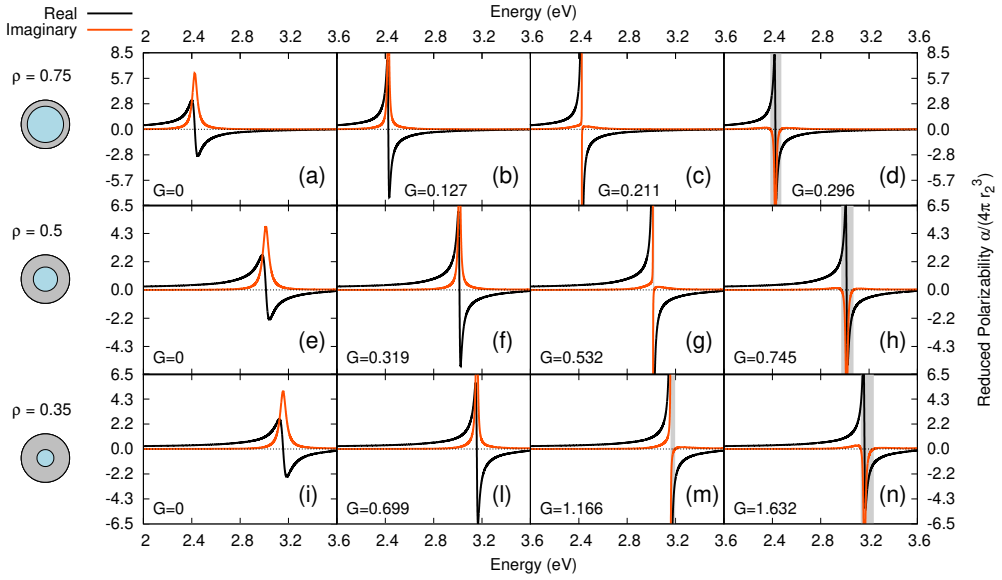

Fig. 4. *Silver nano-shell:* Evolution of the plasmon resonance of a 20-nm nano-shell particle embedding a gain enriched silica core in a silver shell and diluted in water. As gain is increased (from left to right) and for different shell thickness [increasing from up to down] before and after the singular plasmon values [(c), (g), (m)]. Parameters: $\varepsilon_h = 1.769$ (water), $\varepsilon_b = 2.1316$ (silica), $\omega_g = \omega_{sp}$ and $\hbar\Delta = 0.15$ eV. The frequency ranges in which the system becomes emissive ($\alpha''(\omega) < 0$) are highlighted in gray.

with the previous core-shell case. First, as observed in fig. 1, the singular frequency changes significantly as ρ is varied, as is usual with nanoshells. This could allow for some flexibility to position the singular resonance frequency ω_{sp} on the fixed emission center frequency ω_g of any predetermined gain medium, which may prove easier in practice than to find a dye emitting as close as possible to the fixed singular resonance in the case of core-shells. Another advantage of the nanoshell configuration is that the field inside the core keeps uniform, and the plasmonic field outside the particle keeps dipolar, even in the emissive regimes (grey regions in fig. 4c, g, m, d, h, n), leading to single-mode nanolasing. On the contrary, core-shell systems will suffer a "mode cascade mechanism" which will inevitably lead to multi-mode lasing, as was discussed in [37].

5. High-loss metal behavior

As in the case of a single particle in a uniform medium [30], the spectral response of a gold core-shell nanoparticle appears to be richer than its silver counterpart. The first thing one can

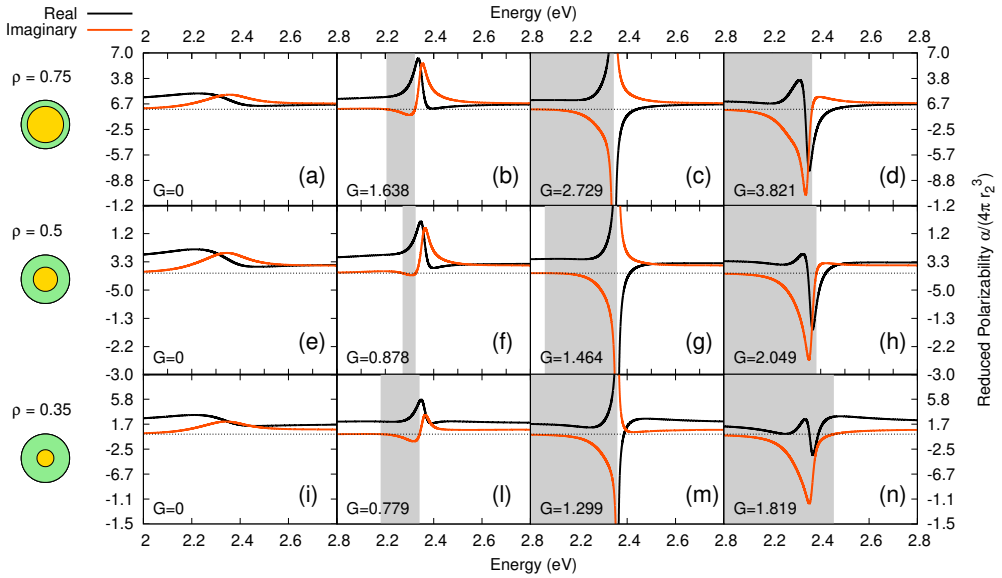

Fig. 5. *Gold core-shell:* Evolution of the plasmon resonance of a 20-nm core-shell nanoparticle embedding a gold-core in a gain enriched silica-shell and dispersed in water. Black curves: real part of the reduced polarizability, orange curves: imaginary part. As gain is increased (from left to right) and for different shell thickness [increasing from up to down] before and after the singular plasmon values [(c), (g), (m)]. Parameters: $\varepsilon_h = 1.769$ (water), $\varepsilon_b = 2.1316$ (silica), $\omega_g = \omega_{sp}$ and $\hbar\Delta = 0.15$ eV. The frequency ranges in which the system becomes emissive ($\alpha''(\omega) < 0$) are highlighted in gray.

notice in figure 5 is that, due to the higher metal losses, the gain threshold G_{th} necessary to produce the singular behavior (fig. 5c, g, m) is around twenty times larger than the one for silver (fig. 3c, g, m), again showing gold a less promising candidate for nanolasing applications than silver. Also, for the same reason, the plasmon resonance in absence of gain (fig. 5a, e, i) is less pronounced compared to that of silver and also much more distorted as an effect of the interband transitions.

The most interesting aspect here is that, the high level of gain necessary to drive any response, produces an additional deformation on the plasmonic resonance even before the singular point (fig. 5b, f, l). When a thick shell is considered and an amount of gain lower than the one needed to drive the singular behavior is added to the system ($G < G_{th}$) as in fig. 5l), we observe a *real* part of the polarizability $\alpha'(\omega)$ having a bell-like shape (whereas this is usually seen for imaginary response), and conversely, the *imaginary* part $\alpha''(\omega)$ has here the sigmoidal shape normally expected for real part. Similar shapes are observed for thicker shells (not shown). This behavior, called "conjugate plasmon" is due to Fano-type resonances, and was theoretically predicted for the first time in the case of a metal particle in a uniform gain medium [30]. Conjugate plasmons show one particularly attractive property: at the plasmon frequency, where the real response is maximal, losses are also close to zero; which is in fact much more favorable for most of practical applications than the situation of usual plasmons.

When thinner shells are considered, the deformed spectral response does not produce an actual swap between the real and the imaginary part of $\alpha(\omega)$, instead, these appear to be quite

symmetrical, still keeping the interesting propriety of having a large, positive real part where the losses are negligible. Moreover, when thin shells are considered and an amount of gain greater than G_{th} is used (fig. 5d, h), an even more interesting symmetrical situation appears: while the conjugate plasmons obtained before the singular point have a positive real part, here they display a negative real part. This type of responses where the real part of α is significant and the imaginary part is negligible, could be extremely valuable, if one is interested in obtaining artificial, low-loss media with so-called "negative" properties. The important setback here is that this is observed for very high (probably irrealistic) gain levels in the system, and also these features lies very close to the emissive spectral region (grey regions in fig. 5b, f, l, d, h), which could limit the possibility to use this propriety for applications.

Finally, quite interestingly, it should be stressed that due to the strong spectral deformations related to high losses and interband transitions, the system becomes emissive for amounts of gain *less* than the threshold gain needed to produce the singular behavior (see the grey regions in fig. 5b, f, l). The exact nature of these "low-gain" emissive states as compared to those obtained for ($G < G_{\text{th}}$) remains to be explored, but paradoxically enough, this indicates that the interband transitions may provide ways to reduce emission with lower gain levels than expected for gold.

We conclude the study of plasmon spectra with figure 6, where the spectral behavior of gold nano-shell structures is presented. Here one can easily see that particles with thin gold shells

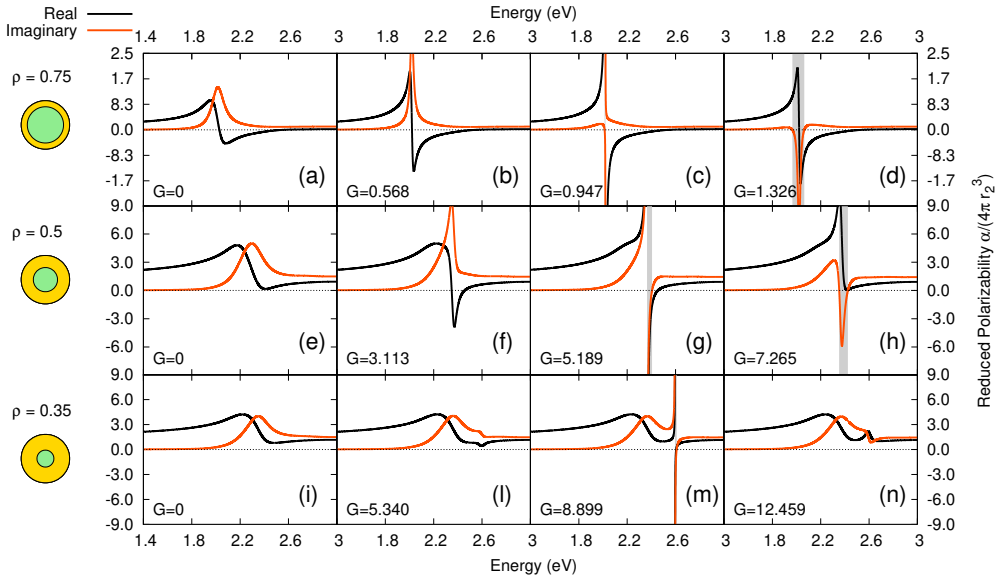

Fig. 6. *Gold nano-shell:* Evolution of the plasmon resonance of a 20-nm nano-shell nanoparticle embedding a gain enriched silica core in a gold shell and dispersed in water. Black curves: real part of the reduced polarizability, orange curves: imaginary part. As gain is increased (from left to right) and for different shell thickness [increasing from up to down] before and after the singular plasmon values [(c), (g), (m)]. Parameters: $\varepsilon_{\text{h}} = 1.769$ (water), $\varepsilon_{\text{b}} = 2.1316$ (silica), $\omega_g = \omega_{\text{sp}}$ and $\hbar\Delta = 0.15$ eV. The frequency ranges in which the system becomes emissive ($\alpha''(\omega) < 0$) are highlighted in gray.

behave basically the same as silver nanoshells (fig. 6a-d). Provided that enough gain is included in the system, the same spectral behavior appears until around $\rho \sim 0.5$. However, as soon as the metal volume fraction increases more, the extremely high level of gain necessary to drive any enhancement in the resonance, produces an additional deformation in the spectra (fig. 6e-n), up to the point where the losses are so high that, even if we still observe a singular behavior

(fig. 6m), any emission seems to be lost for larger quantities of gain (fig. 6n). In such situations where extreme gain competes with extreme losses, other physical effects (not included in this model) may rise; for this reason, we would definitely suggest caution in acquiring the spectral results presented in figs. 6i-n.

6. Density of gain elements (emitters)

It is of prime importance, for the reasons mentioned in the last paragraph and others, to provide a way to quantitatively evaluate if a gain level is realistically attainable or not. For this reason one has to relate the G parameter of equation 2 with real physical quantities. There are different approaches to do this: here we solve the time dynamical model for gain elements based on the optical Bloch equations we presented in a previous work [37], looking for the steady state regime. The result of this calculation gives:

$$\varepsilon_g = \varepsilon_\mathrm{b} + \frac{2n\mu^2 N}{3\hbar\varepsilon_0[2(\omega-\omega_\mathrm{g})+i\Delta]} \tag{14}$$

We remind the reader that n is the volume density of gain elements (emitters such as dye molecules, quantum dots, etc.), μ the transition dipole moment of the emitters, N is the population inversion (i. e. the pumped fraction of the of the gain elements population) and $\hbar$ the reduced Plank constant. Comparing equation 14 with equation 2, we get the equation 3 presented in the beginning of this article, that is:

$$G = \frac{2n\mu^2}{3\hbar\varepsilon_0\Delta}\tilde{N}.$$

From the latter, one can calculate the volume density n of emitters:

$$n = \frac{3\hbar\varepsilon_0\Delta}{2\mu^2 N}G, \tag{15}$$

which gives a relation between the gain level G in the system and the required emitter density n to generate it. It also allows to calculate the emitter density n_th necessary to reach the lasing threshold $G = G_\mathrm{th}$ and produce a singular resonance as:

$$n_\mathrm{th}(\rho) = \frac{3\hbar\varepsilon_0\Delta}{2\mu^2 N}G_\mathrm{th}(\rho), \tag{16}$$

It is worth recalling that, as discussed previously, in order for G_th (and thus for n_th) to be only function of ρ, one has to align the gain element center-line emission with the plasmon resonance ($\omega_\mathrm{g} = \omega_\mathrm{sp}$); moreover if we consider a fully pumped nanoparticle ($\tilde{N} = 1$), all of the constants in equation 16 are already set but the transition dipole moment μ. In the following characterization, we plot n_th as a function of the aspect ratio ρ, considering dyes with transition dipole moments in the range $\mu = 10 \pm 5$ D, comparable to the classical dye Rhodamine 123 ($\mu_R \sim 8.1$ D) [41].

The results of this characterization are presented in figure 7 for core-shell and in figure 8 for nano-shell structures. In both figures, the continuous lines (resp. black line for silver, and orange line for gold) are calculated for $\mu = 10D$, while the shaded areas (resp. yellow for gold and grey for silver) show how n_th changes by varying μ in the interval 5 D $\leq \mu \leq$ 15 D (the lowest border corresponds to the highest μ). For reference, we also compared the found densities with the density of the close-packing of spheres in a dense arrangement [42], $n_\mathrm{CP} = 0.74$: this is materialized by a red horizontal line, above which emitters density are geometrically prohibited. This should be understood as a mere indication of maximum densities, since the gain medium is expected to structurally collapse well before the geometrical limit, as the host matrix (e.g., silica) is gradually replaced by emitters. Also, at high densities, even before two gain elements

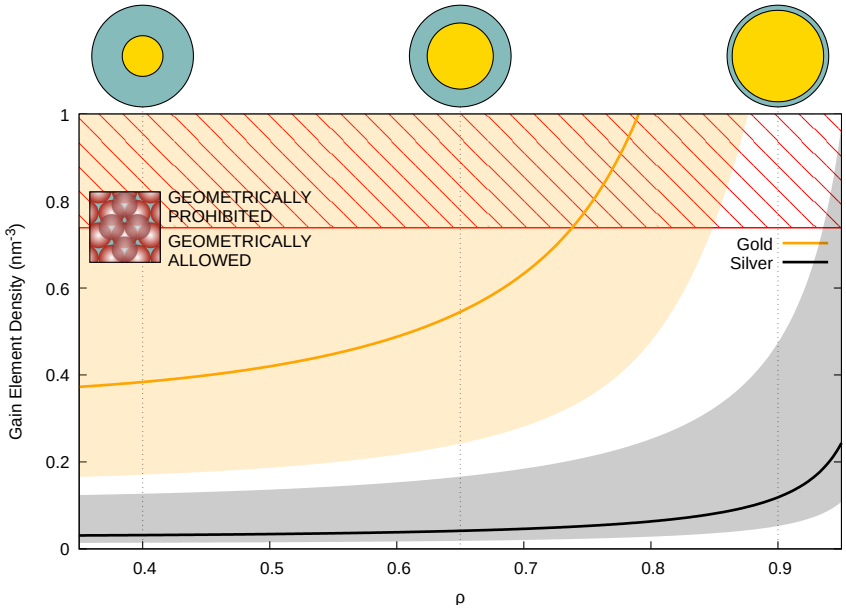

Fig. 7. Threshold emitter density n_{th} as a function of the aspect ratio ρ for a core-shell structure. *orange line:* Gold core. The continuous line refers to $\mu = 10$ D, the yellow shaded area to the interval 5 D $\leq \mu \leq$ 15 D (see main text). *Black line:* Silver core. The continuous line refers to $\mu = 10$ D, the grey shaded area to the interval 5 D $\leq \mu \leq$ 15 D (see main text). The horizontal red line corresponds to the dense packing limit for spheres.

physically touch each other, emitter-emitter couplings can become strongly detrimental for their efficiency [43–46].

The first thing one can appreciate in figure 7 is that, no matter if using a gain element with transition dipole moment as low as $\mu = 5$ D it is still possible to fit enough elements to drive a singular behavior up to very thin shells. On the other hand, when gold is used, due to stronger metallic losses, low transition dipole moments do not allow singular behavior with realistic emitter densities; even with $\mu = 10$ D, it is necessary to have enough gain, i.e. thick enough shells, to allow for it ($\rho \lesssim 0.65$).

In figure 8 we present the same characterization for nano-shell particles. Here one has to consider that the higher metal volume fraction is for thick shells (low ρ) and consequently, the particle density needed to produce the singular behavior gets lower for higher ρ (thin shells). One can observe ripples, which are again due to measurements discrepancies in the low-energy end of the silver permittivity data we used [32]. If one compares the behavior for a silver nano-shell (fig. 8: black continuous line) with the one of a nano-shell made of gold (fig. 8: orange continuous line), it is evident once again that, due to the lower losses in silver, it is possible to use a wider range of shell thicknesses and still be able to fit enough gain in the core to produce a singular behavior: even with a gain element with a relatively low transition dipole moment one can, in principle, still obtain emission with thick-shell-particles ($\rho \sim 0.5$). Also, when using gain elements with a transition dipole moment of around 10 D it appears to be possible to realize an emissive silver nano-shell up to very thick shells ($\rho \lesssim 0.3$).

Finally, we can confirm here what we anticipated when discussing fig. 6: it appears to be impossible to fit enough gain in the core of a gold nano-shell particle with a thick shell ($\rho \lesssim 0.5$), even when using high transition dipole moment ($\mu \sim 15$ D) gain elements. This means that,

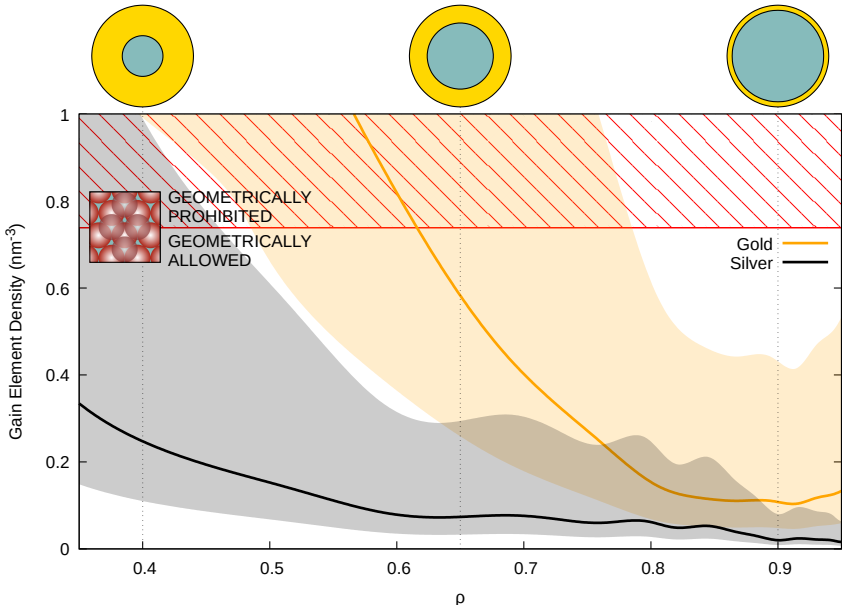

Fig. 8. Threshold emitter density n_{th} as a function of the aspect ratio ρ for a nano-shell structure. *Orange line:* Gold shell. The continuous line refers to $\mu = 10$ D, the yellow shaded area to the interval $5\text{ D} \leq \mu \leq 15\text{ D}$ (see main text). *Black line:* Silver shell. The continuous line refers to $\mu = 10$ D, the grey shaded area to the interval $5\text{ D} \leq \mu \leq 15\text{ D}$ (see main text). The horizontal red line corresponds to the dense packing limit for spheres.

unless a new gain element with an extraordinary transition dipole moment is developed, the spectra presented in figure 6e-n for gold are not realistically realizable.

Summarizing, when silver is used, it appears that both the core-shell and the nano-shell are viable candidates to realize a plasmonic emitter; when gold is used, nano-shells are a better solution unless very-high-transition-dipole gain elements are employed. Finally, in the pursuit for the ideal gain element, size is a hidden factor that might not be evident in our characterization: the gain element radius is in fact relevant because, as an example, high transition dipole moment quantum dots tend to have typical diameter ranging between 2 and 10 nm [47, 48], and may be too big to reach high packing densities, or to even fit in small nanoparticles (like the ones we focused on), requiring large, multipolar ones instead.

7. Designing a gain-assisted nanoparticle for singular resonance

We will now harvest from our characterization a step by step procedure to facilitate the design of a gain assisted nanoparticle including enough gain to allow a singular resonance.

- Firstly one can use equation 12 to calculate the singular plasmon frequency when $\omega_{\text{g}} = \omega_{\text{sp}}$ or (and this is especially effective for nano-shells) set the desired singular frequency ω_{sp} and use the same equation to determine the right radius ratio ρ;

- once ω_{sp} is set, one has to look for a gain element whose emission central frequency is the closest possible to it ($\omega_{\text{g}} \sim \omega_{\text{sp}}$) to maximize the coupling efficiency;

- if the found gain emission frequency is different from the singular plasmon frequency ($\omega_{\text{g}} \neq \omega_{\text{sp}}$), one can use equation 10 to calculate the new singular frequency and equation 11

to calculate the threshold gain G_{th}, else (if $\omega_g = \omega_{sp}$) one can directly use equation 13 to calculate G_{th};

- knowing G_{th}, one can use equation 16 to calculate the threshold particle density to be included in the shell (core-shells) or in the core (nano-shells) to allow for a singular resonance when completely pumped.

It is of prime importance to stress here that, at this stage, the presented procedure is not meant to be taken as a recipe or as a validated protocol, but more as an indication of the most promising direction to be explored in order to experimentally test our findings.

8. Conclusions

We have studied the plasmonic response of metal nanoparticles in the core-shell and nano-shell configurations, when pumped gain elements are added to the system. The findings of this simple, steady state approach can be validated using a more complex, dynamical, multipolar model (as the one we presented in a previous work [37]) until the gain threshold needed to overcompensate the metal losses and driven emission is reached.

Taking advantage of the simplicity of this model, we generalized a method allowing to calculate both the threshold gain G_{th} and the singular resonance frequency ω_{sp} (nanolasing frequency) for both core-shell and nano-shell particles. When the efficiency of the coupling between the gain elements and the plasmon is maximized (by superimposing the gain emission line with the plasmonic resonance $\omega_g = \omega_{sp}$), both the singular resonance frequency and the threshold gain are only function of ρ. We used this simplified dependency to characterize the evolution of the plasmonic spectral shape as a function of the gain added for both core-shells and nano-shells made in gold and silver, we discussed up to what point these spectra are reliable, where and when this model breaks and what one can expect when it does.

This way we have shown that the quality of the resonances can be drastically enhanced until the response can become singular at G_{th}, this is especially true for metals with a low level of losses like silver, where additional gain only produces an increasing quality of the plasmon resonance towards the singular point, without introducing any additional deformation in the spectral shape. In gold, due to the higher loss associated with the interband transition, the situation is richer. Deformed spectra as the "conjugate" plasmon appear revealing spectral responses that, if realizable, could be harbingers of novel applications.

We discussed that, when the imaginary part of the polarizability gets negative, one can expect emission in that frequency range; and also mentioned that, when this happens, a quantitative description of the phenomenon falls out of the scope of our model.

Finally we proposed a way to determine if a gain level G is realistic or not, by translating it in terms of particle density n and comparing this last to the close-packing of equal spheres is a dense arrangement, this way we have shown that depending on the transition dipole moment μ of the used gain, some configuration are more realistic than others and, as expected, silver nanoparticles sporting the lowest possible metal volume-ratio are better candidates for the realization of an emitting plasmonic nanoparticle. Eventually, we reorganized all of our findings in a step by step procedure aimed to facilitate the synthesis of nanoparticles which could potentially being driven to emission.

The presented model is general and it can be easily customized to describe a wider range of different materials and configuration. Fine tuning, using different particle sizes and gain elements, can easily be done allowing the possibility to design different nanostructures optimized for diverse cutting edge optical applications.

9. Disclosures

The authors declare no conflicts of interest.

10. Data availability

Data underlying the results presented in this paper are not publicly available at this time but may be obtained from the authors upon reasonable request.

References

1. S. A. Ramakrishna and J. B. Pendry, "Removal of absorption and increase in resolution in a near-field lens via optical gain," Phys. Rev. B **67**, 201101.1–201101.4 (2003).
2. N. M. Lawandy, "Localized Surface Plasmon Singularities in Amplifying Media," Appl. Phys. Lett. **85**, 5040–5042 (2004).
3. M. A. Noginov, G. Zhu, M. Bahoura, J. Adegoke, C. E. Small, B. A. Ritzo, V. P. Drachev, and V. M. Shalaev, "Enhancement of surface plasmons in an Ag aggregate by optical gain in a dielectric medium," Opt. Lett. **31**, 3022–3024 (2006).
4. M. Wegener, J. García-Pomar, C. Soukoulis, N. Meinzer, M. Ruther, and S. Linden, "Toy model for plasmonic metamaterial resonances coupled to two-level system gain," Arxiv preprint arXiv:0809.0487 (2008).
5. A. Fang, T. Koschny, and C. Soukoulis, "Self-consistent calculations of loss-compensated fishnet metamaterials," Phys. Rev. B **82**, 121102 (2010).
6. S. Xiao, V. Drachev, A. Kildishev, X. Ni, U. Chettiar, H. Yuan, and V. Shalaev, "Loss-free and active optical negative-index metamaterials," Nature **466**, 735–738 (2010).
7. A. Chipouline, J. Petschulat, A. Tuennermann, T. Pertsch, C. Menzel, C. Rockstuhl, F. Lederer, and V. A. Fedotov, "Multipole model for metamaterials with gain: from nano-laser to quantum metamaterials," in *Metamaterials VI,* vol. 8070 V. Kuzmiak, P. Markos, and T. Szoplik, eds., International Society for Optics and Photonics (SPIE, 2011), pp. 123 – 131.
8. S. Liu, J. Li, F. Zhou, L. Gan, and Z. Li, "Efficient surface plasmon amplification from gain-assisted gold nanorods," Opt. letters **36**, 1296–1298 (2011).
9. S. Wuestner, A. Pusch, K. Tsakmakidis, J. Hamm, and O. Hess, "Overcoming losses with gain in a negative refractive index metamaterial," Phys. review letters **105**, 127401 (2010).
10. P. Bolger, W. Dickson, A. Krasavin, L. Liebscher, S. Hickey, D. Skryabin, and A. Zayats, "Amplified spontaneous emission of surface plasmon polaritons and limitations on the increase of their propagation length," Opt. letters **35**, 1197–1199 (2010).
11. N. Meinzer, M. Ruther, S. Linden, C. Soukoulis, G. Khitrova, J. Hendrickson, J. Olitsky, H. Gibbs, and M. Wegener, "Arrays of Ag split-ring resonators coupled to InGaAs single-quantum-well gain," Arxiv preprint arXiv:1009.0693 (2010).
12. A. Sarychev and G. Tartakovsky, "Magnetic plasmonic metamaterials in actively pumped host medium and plasmonic nanolaser," Phys. Rev. B **75**, 085436 (2007).
13. R. F. Oulton, V. J. Sorger, T. Zentgraf, R. Ma, C. Gladden, L. Dai, G. Bartal, and X. Zhang, "Plasmon lasers at deep subwavelength scale," Nature **461**, 629–632 (2009).
14. J. Zhou, T. Koschny, and C. M. Soukoulis, "An efficient way to reduce losses of left-handed metamaterials." Opt. Express **16**, 11147–52 (2008).
15. G. Strangi, A. De Luca, S. Ravaine, M. Ferrie, and R. Bartolino, "Gain induced optical transparency in metamaterials," Appl. Phys. Lett. **98**, 251912 (2011).
16. A. De Luca, M. P. Grzelczak, I. Pastoriza-Santos, L. M. Liz-Marzán, M. L. Deda, M. Striccoli, and G. Strangi, "Dispersed and Encapsulated Gain Medium in Plasmonic Nanoparticles: a Multipronged Approach to Mitigate Optical Losses," ACS Nano **5**, 5823–5829 (2011).
17. D. Schurig, J. J. Mock, B. J. Justice, S. A. Cummer, J. B. P. ans A. F. Starr, and D. R. Smith, "Metamaterial Electromagnetic Cloak at Microwave Frequencies," Science **314**, 977–980 (2006).
18. W. Cai, U. K. Chettiar, A. V. Kildishev, and V. M. Shalaev, "Optical Cloaking with Metamaterials," Nat. Photon. **1**, 224–227 (2008).
19. A. Veltri, "Designs for electromagnetic cloaking a three-dimensional arbitrary shaped star-domain." Opt. express **17**, 20494–501 (2009).
20. M. A. Noginov, G. Zhu, A. M. Belgrave, R. Bakker, V. M. Shalaev, E. E. Narimanov, S. Stout, E. Herz, T. Suteewong, and U. Wiesner, "Demonstration of a spaser-based nanolaser," Nature **460**, 1110–1112 (2009).
21. E. Plum, V. Fedotov, P. Kuo, D. Tsai, and N. Zheludev, "Towards the lasing spaser: controlling metamaterial optical response with semiconductor quantum dots," Opt. Express **17**, 8548–8550 (2009).
22. N. Zheludev, S. Prosvirnin, N. Papasimakis, and V. Fedotov, "Lasing Spaser," Nat. Photon. **2**, 351–354 (2008).
23. M. I. Stockman, "Spasers explained," Nat. Photonics **2**, 327–329 (2008).
24. C. Graf and A. van Blaaderen, "Metallodielectric Colloidal Core-Shell Particles for Photonic Applications," Langmuir **18**, 524–534 (2002).
25. O. G. Tovmachenko, C. Graf, D. J. van den Heuvel, A. van Blaaderen, and H. C. Gerritsen, "Fluorescence Enhancement by Metal-Core/Silica-Shell Nanoparticles," Adv. Mat. **18**, 91–95 (2006).
26. X. Meng, K. Fujita, S. Murai, T. Matoba, and K. Tanaka, "Plasmonically Controlled Lasing Resonance with Metallic-Dielectric Core-Shell Nanoparticles," NanoLett. **11**, 1374–1378 (2011).

27. A. De Luca, M. Ferrie, S. Ravaine, M. La Deda, M. Infusino, A. Rashed, A. Veltri, A. Aradian, N. Scaramuzza, and G. Strangi, "Gain functionalized core-shell nanoparticles: the way to selectively compensate absorptive losses," J. Mater. Chem. (2012).
28. V. Ponsinet, A. Aradian, P. Barois, and S. Ravaine, "Self-Assembly and Nanochemistry Techniques for the Fabrication of Metamaterials," in *Metamaterials Handbook vol.2: Applications of Metamaterials,* F. Capolino, ed. (CRC Press, 2009), pp. 32–1 – 32–39.
29. A. Aradian, P. Barois, O. Mondain-Monval, V. Ponsinet, and A. Baron, "The Bottom-Up Approach toward Artificial Optical Magnetism in Metastructures," in *Hybrid Flatland Metastructures,* R. Caputo and G. E. Lio, eds. (AIP Publishing, 2021), pp. 3–1 – 3–28.
30. A. Veltri and A. Aradian, "Optical response of a metallic nanoparticle immersed in a medium with optical gain," Phys. Rev. B **85**, 115429 (2012).
31. J. D. Jackson, *Classical Electrodynamics* (Wiley, New York, 1998), 3rd ed.
32. P. B. Johnson and R. W. Christy, "Optical Constants of the Noble Metals," Phys. Rev. B **6**, 4370–4379 (1972).
33. V. Caligiuri, L. Pezzi, A. Veltri, and A. De Luca, "Resonant Gain Singularities in 1D and 3D Metal/Dielectric Multilayered Nanostructures," ACS Nano **11**, 1012–1025 (2017).
34. M. Infusino, A. De Luca, A. Veltri, C. Vázquez-Vázquez, M. Correa-Duarte, R. Dhama, and G. Strangi, "Loss-Mitigated Collective Resonances in Gain-Assisted Plasmonic Mesocapsules," ACS Photonics **1**, 371–376 (2014).
35. P. Polimeno, F. Patti, M. Infusino, J. J. Sanchez, M. A. Iati, R. Saija, G. Volpe, O. M. Marago, and A. Veltri, "Gain-Assisted Optomechanical Position Locking of Metal/Dielectric Nanoshells in Optical Potentials," ACS Photonics (2020).
36. P. Polimeno, F. Patti, M. Infusino, M. A. Iatì, R. Saija, G. Volpe, O. M. MaragÒ, and A. Veltri, "Optical trapping of gain-assisted plasmonic nano-shells: theorical study of the optical forces in a pumped regime below the emission threshold," in *Optical Trapping and Optical Micromanipulation XVIII,* vol. 11798 K. Dholakia and G. C. Spalding, eds., International Society for Optics and Photonics (SPIE, 2021), pp. 170 – 177.
37. A. Veltri, A. Chipouline, and A. Aradian, "Multipolar, time-dynamical model for the loss compensation and lasing of a spherical plasmonic nanoparticle spaser immersed in an active gain medium," Sci. Reports **6**, 33018 (2016).
38. D. Baranov, E. Andrianov, A. Vinogradov, and A. Lisyansky, "Exactly solvable toy model for surface plasmon amplification by stimulated emission of radiation," Opt. express **21**, 10779–91 (2013).
39. E. Prodan and P. Nordlander, "Structural tunability of the plasmon resonances in metallic nanoshells," Nano Lett. **3**, 543–547 (2003).
40. A. Veltri, A. Aradian *et al.*, to be published .
41. P.-H. Chung, C. Tregidgo, and K. Suhling, "Determining a fluorophore's transition dipole moment from fluorescence lifetime measurements in solvents of varying refractive index," Methods Appl. Fluoresc. **4**, 045001 (2016).
42. Wikipedia contributors, "Close-packing of equal spheres — Wikipedia, the free encyclopedia," (2021). [Online; accessed 20-July-2021].
43. P. Andrew and W. L. Barnes, "Forster energy transfer in an optical microcavity," Science **290**, 785–788 (2000).
44. J. Zhang, Y. Fu, M. H. Chowdhury, and J. R. Lakowicz, "Enhanced Forster Resonance Energy Transfer on Single Metal Particle," J. Chem. Phys. **111**, 50–56 (2007).
45. X. Zhang, C. A. Marocico, M. Lunz, V. A. Gerard, Y. K. Gun'Ko, V. Lesnyak, N. Gaponik, A. S. Susha, A. L. Rogach, and A. L. Bradley, "Experimental and theoretical investigation of the distance dependence of localized surface plasmon coupled förster resonance energy transfer," ACS Nano **8**, 1273–1283 (2014).
46. P. Ghenuche, M. Mivelle, J. De Torres, S. B. Moparthi, H. Rigneault, N. F. Van Hulst, M. F. García-Parajó, and J. Wenger, "Matching Nanoantenna Field Confinement to FRET Distances Enhances Förster Energy Transfer Rates," Nano Lett. **15**, 6193–6201 (2015).
47. S. I. Pokutnyi, Y. N. Kulchin, and V. P. Dzyuba, "Optical absorption of one-particle electron states in quasi-zero-dimensional nanogeterostructures: Theory," Pac. Sci. Rev. A: Nat. Sci. Eng. **18**, 261–265 (2016).
48. Wikipedia contributors, "Close-packing of equal spheres — Wikipedia, the free encyclopedia," (2021). [Online; accessed 23-July-2021].